OsteoArthritis and Cartilage (2004) **12,** 177–190

doi:10.1016/j.joca.2003.11.003

Osteoarthritis and Cartilage

International Cartilage Repair Society

OARSI OSTEOARTHRITIS RESEARCH SOCIETY INTERNATIONAL

Whole-Organ Magnetic Resonance Imaging Score (WORMS) of the knee in osteoarthritis

C. G. Peterfy M.D. Ph.D.†*, A. Guermazi M.D.†, S. Zaim M.D.†, P. F. J. Tirman M.D.‡, Y. Miaux M.D.†, D. White Ph.D.†, M. Kothari Ph.D.†, Y. Lu Ph.D.§, K. Fye M.D.§, S. Zhao Ph.D.§ and H. K. Genant M.D.§

† *Synarc, Inc., San Francisco, CA, USA*

‡ *National Orthopedic Imaging Associates, San Francisco, CA, USA*

§ *Osteoporosis & Arthritis Research Group, University of California, San Francisco, CA, USA*

Summary

Objectives: To describe a semi-quantitative scoring method for multi-feature, whole-organ evaluation of the knee in osteoarthritis (OA) based on magnetic resonance imaging (MRI) findings. To determine the inter-observer agreement of this scoring method. To examine associations among the features included in the scoring method.

Methods: Nineteen knees of 19 patients with knee OA were imaged with MRI using conventional pulse sequences and a clinical 1.5 T MRI system. Images were independently analyzed by two musculoskeletal radiologists using a whole-organ MRI scoring method (WORMS) that incorporated 14 features: articular cartilage integrity, subarticular bone marrow abnormality, subarticular cysts, subarticular bone attrition, marginal osteophytes, medial and lateral meniscal integrity, anterior and posterior cruciate ligament integrity, medial and lateral collateral ligament integrity, synovitis/effusion, intraarticular loose bodies, and periarticular cysts/bursitis. Intraclass correlation coefficients (ICC) were determined for each feature as a measure of inter-observer agreement. Associations among the scores for different features were expressed as Spearman Rho.

Results: All knees showed structural abnormalities with MRI. Cartilage loss and osteophytes were the most prevalent features (98% and 92%, respectively). One of the least common features was ligament abnormality (8%). Inter-observer agreement for WORMS scores was high (most ICC values were >0.80). The individual features showed strong inter-associations.

Conclusion: The WORMS method described in this report provides multi-feature, whole-organ assessment of the knee in OA using conventional MR images, and shows high inter-observer agreement among trained readers. This method may be useful in epidemiological studies and clinical trials of OA.

Key words: Osteoarthritis, Cartilage, MRI, Imaging, Scoring.

Introduction

The structural determinants of pain and mechanical dysfunction in osteoarthritis (OA) are not well understood, but are believed to involve multiple interactive pathways[1–4]. Accordingly, OA is best modeled as a disease of organ failure, in which injury to one joint component leads to damage of other components, and collectively to joint failure and the clinical manifestations of OA. The current practice of monitoring only a few features – typically radiographic joint-space narrowing and osteophytes – therefore provides only a keyhole view of this disease process, and is limited in content validity as an assessment of disease severity. A broader panel of imaging markers, i.e., a whole-organ evaluation, is needed to evaluate properly the structural integrity of joints affected by OA.

*Address correspondence to: Charles Peterfy, M.D., Ph.D., Chief Medical Officer, Executive Vice President, Synarc, Inc., 575 Market Street, 17th Floor, San Francisco, CA 94105, USA. Tel.: +1-415-817-8901; Fax: +1-415-817-8999; E-mail: charles.peterfy@synarc.com

Received 21 April 2003; revision accepted 2 November 2003.

Radiography, while offering high contrast and resolution for cortical and trabecular bone, cannot directly visualize non-ossified joint structures, such as articular cartilage, marrow tissue, menisci, cruciate and collateral ligaments, synovial fluid, and periarticular tendons and muscles, and therefore lacks the scope required for whole-organ assessment of joints[5]. Moreover, morphological distortion, geometric magnification and superimposition of overlying structures caused by the projectional viewing perspective of radiography complicate dimensional measurements, and can obscure important findings. Magnetic resonance imaging (MRI), on the other hand, is ideally suited for imaging arthritic joints. Not only is it free of ionizing radiation, but its tomographic viewing perspective obviates morphological distortion, magnification and superimposition. More importantly, however, MRI is unparalleled in its ability to discriminate articular tissues, such as cartilage, menisci and ligaments, and therefore holds the greatest potential as a tool for whole-organ imaging of the joint.

In this article, we present a semiquantitative, multi-feature scoring method (WORMS) for whole-organ evaluation of the knee that is applicable to conventional MRI techniques that are widely available and easy to

implement at most imaging centers and hospitals around the world.

Methods

SUBJECTS

Nineteen consecutive patients (15 men, 4 women; age 61 years±8 years) with symptomatic OA of the knee were recruited from the rheumatology clinic of the University of California San Francisco Medical Center. All patients complained of pain in the study knee (ten right, nine left) for at least half the days of the preceding month. None of the patients had a history of previous knee trauma, knee surgery or arthroscopy. Conventional standing, extended-joint radiographs of the knees showed changes of Kellgren–Lawrence grade 2 (*N*=4) to 3 (*N*=15) and a mean minimum medial femorotibial joint-space width of 2.2 mm (range=0.5 mm–4.5 mm, S.D.=1.3 mm, measured manually with a graduated lens by an experienced clinical-trials radiologist). Fourteen patients were taking analgesics. Five were not receiving any medication. The study protocol was approved by institutional board review and informed consent was obtained from each subject prior to enrollment.

MRI

MRI of the study knee of each patient was acquired with a 1.5 Tesla whole-body scanner using a commercial circumferential knee coil. Imaging sequences included, axial T1-weighted spin-echo (SE: 700/11 [TR msec/TE msec], 20 cm field of view [FOV], 5 mm/1 mm [slice thickness/interslice gap], 256×192 matrix, frequency encoding [FE] anterior-posterior, one excitation), coronal T1-weighted SE (600/11, 16 cm FOV, 4 mm/0.5 mm, 256×192, FE superior-inferior, two excitations averaged), sagittal T1-weighted SE (600/11, 16 cm FOV, 4 mm/0.5 mm, 256×192, FE anterior-posterior, two excitations averaged), sagittal T2-weighted fast spin echo (FSE: 2500/90; echo train length (ETL) of eight; 14 cm FOV, 4 mm/0 mm, 256×192, FE superior-inferior, two excitation averaged) with fat suppression (frequency-selective presaturation), and sagittal fat-suppressed T1-weighted three dimensional (3D) spoiled gradient echo (FS-3DSPGR: 58/6, 40° flip angle, 14 cm FOV, 256×128 matrix, 60 contiguous 2-mm slices covering all articular cartilage plates in the knee, FE, superior-inferior, one excitation, frequency-selective fat saturation, superior-inferior saturation bands to minimize pulsation artifacts). The total time required for MRI, including patient set up, was 60 min.

WHOLE-ORGAN MRI SCORING (WORMS)

All images were transferred to a Sun Workstation and analyzed using MRVision software (MRVision, Inc, Menlo Park, CA). Images were scored with respect to 14 independent articular features: cartilage signal and morphology, subarticular bone marrow abnormality, subarticular cysts, subarticular bone attrition, marginal osteophytes, medial and lateral meniscal integrity, anterior and posterior cruciate ligament integrity, medial and lateral collateral ligament integrity, synovitis, loose bodies and periarticular cysts/bursae. Readings were performed independently by two musculoskeletal radiologists (CP, PT) following two separate two-hour training sessions using different case material than the 19 subjects included in this study. Readers used all images to evaluate each feature.

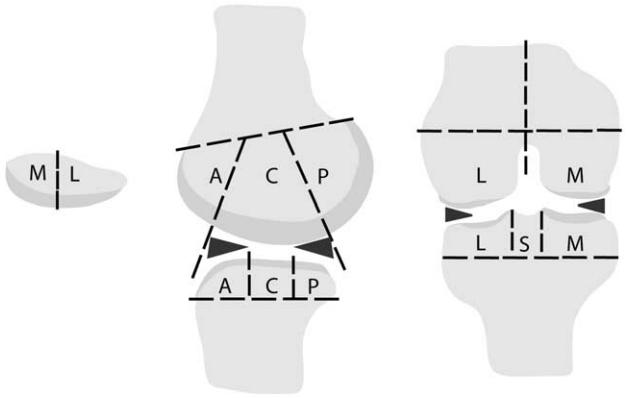

Fig. 1. Regional subdivision of the articular surfaces. The patella (left image) is divided into medial (M) and lateral (L) regions, with the ridge considered part of the M region. The femur and tibia are also divided into M and L regions (right image), with the trochlear groove of the femur considered part of the M region. Region S represents the portion of the tibia beneath the tibial spines. The femoral and tibial surfaces are further subdivided into anterior (A), central (C) and posterior (P) regions (middle image). Region A of the femur corresponds to the patellofemoral articulation; region C the weight bearing surface, and region P the posterior convexity that articulates only in extreme flexion. Region C of the tibial surface corresponds to the uncovered portion between the anterior and posterior horns of the meniscus centrally and the portion covered by the body of the meniscus peripherally.

Five of the features examined (cartilage signal and morphology, subarticular bone marrow abnormality, subarticular cysts, subarticular bone attrition, marginal osteophytes) related to the articular surfaces. These features were evaluated in 15 different regions subdivided by anatomical landmarks in the fully extended knee (Fig. 1). Subdivisions were determined independently by each reader. The patella was divided into the lateral facet (LP) and medial facet (MP). The patellar ridge was considered part of the MP. The subchondral component of each patellar region extended the full thickness of the bone to the opposite cortex. The femoral articular surface was divided into medial (MF) and lateral (LF) condyles, with the trochlear groove considered part of MF. The boundary between MF and LF was defined by a plane aligned with the lateral wall of the femoral notch (Fig. 2). MF and LF were each divided into three regions: (1) anterior (*a*): extending from the anterior-superior osteochondral junction to the anterior margin of the anterior horn of the meniscus; (2) central (*c*): extending from the anterior margin of the anterior horn of the meniscus to the posterior capsular attachment of the posterior horn of the meniscus; and (3) posterior (*p*): extending from the posterior capsular attachment of the posterior horn of the meniscus to the posterior-superior osteochondral junction. The subchondral component of each femoral region extended perpendicularly from the articular surface to the level of an imaginary line connecting the anterior and posterior osteochondral junctions. The medial tibial plateau (MT) and lateral tibial plateau (LT) were each divided into three equal regions: anterior (*a*), central (*c*) and posterior (*p*). Based on these subdivisions, the patellofemoral joint (PFJ) comprised regions MP, LP, MFa and LFa; the medial femorotibial joint (MFTJ) comprised regions MFc, MFp, MTa, MTc and MTp; and the lateral femorotibial joint (LFTJ) comprised regions LFc, LFp, LTa, LTc and LTp. The non-articulating portion of the

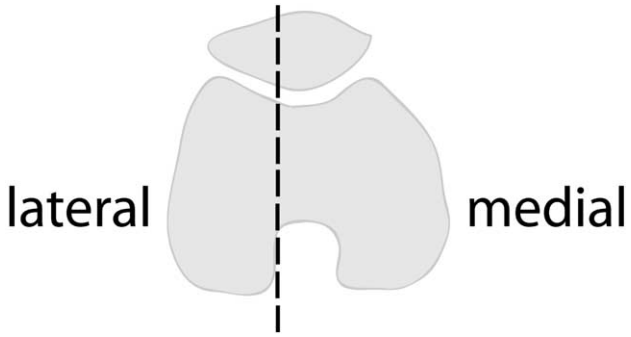

Fig. 2. Defining anterior-lateral femoral region. The medial border of the lateral condyle on an axial image marks the boundary between regions FMa and FLa.

tibial plateau beneath the tibial spines was designated region 'S' (subspinous). The subchondral component of each tibial region extended 2 cm beneath the articular surface.

Cartilage signal and morphology was scored in each of the 14 articular-surface regions (excluding region S) using the fat-suppressed T2-weighted FSE images and the FS-3D SPGR images with an eight-point scale (Fig. 3): 0=normal thickness and signal; 1=normal thickness but increased signal on T2-weighted images; 2.0=partial-thickness focal defect <1 cm in greatest width; 2.5=full-thickness focal defect <1 cm in greatest width; 3=multiple areas of partial-thickness (Grade 2.0) defects intermixed with areas of normal thickness, or a Grade 2.0 defect wider than 1 cm but <75% of the region; 4=diffuse (≥75% of the region) partial-thickness loss; 5=multiple areas of full-thickness loss (grade 2.5) or a grade 2.5 lesion wider than 1 cm but <75% of the region; 6=diffuse (≥75% of the region) full-thickness loss. The maximum cartilage scores for MFTJ, LFTJ, PFJ and the entire knee were 30, 30, 24 and 84, respectively (Table I).

Subarticular bone marrow abnormality was defined as poorly marginated areas of increased signal intensity in the normally fatty epiphyseal marrow on fat-suppressed T2-weighted FSE images. This feature was graded in each of the 14 articular surface regions as well as the region of the tibia beneath the tibial spines (S) from 0 to 3 based on the extent of regional involvement (Fig. 4): 0=none; 1=<25% of the region; 2=25% to 50% of the region; 3=>50% of the region. The maximum scores for MFTJ, LFTJ, PFJ, region S and the entire knee were 15, 15, 12, 3 and 45 respectively (Table I).

Subarticular cysts were identified as foci of markedly increased signal in the subarticular bone with sharply defined, rounded margins and no evidence of internal marrow tissue or trabecular bone on the fat-suppressed T2-weighted FSE images. Bone cysts were graded in each region, including the subspinous region of the tibia (S), from 0 to 3 based on the extent of regional involvement, as for bone marrow abnormality (Fig. 5): 0=none; 1=<25% of the region; 2=25% to 50%of the region; 3=>50% of the region.

Table I
Maximum scores attainable with WORMS

	MFTJ	LFTJ	PFJ	S Region	Total
Cartilage	30	30	24		84
Marrow abnormality	15	15	12	3	45
Bone cysts	15	15	12	3	45
Bone attrition	15	15	12		42
Osteophytes	35	35	28		98
Compartment total	110	110	88		
Menisci	6	6			12
Ligaments					3
Synovitis					3
Total					332

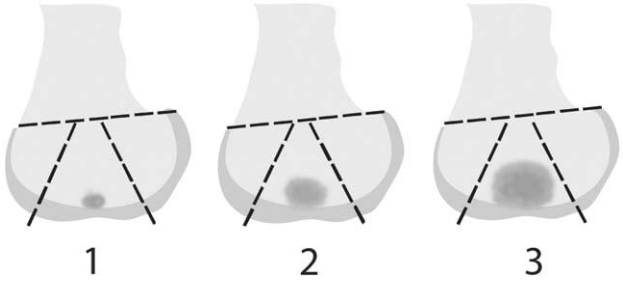

Fig. 4. Subarticular marrow abnormality score. This score is based on the extent of regional marrow involvement by areas of free water signal with ill-defined margins.

Fig. 3. Eight-point scale for scoring articular cartilage signal and morphology. Each region of the knee surface is scored independently.

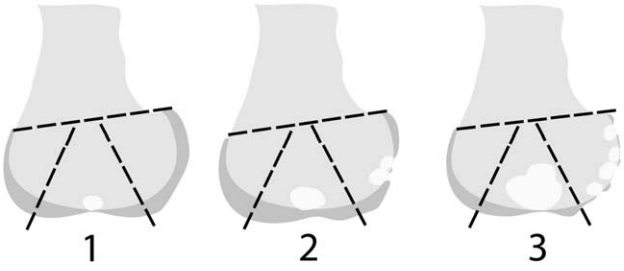

Fig. 5. Subarticular cyst score. Subarticular cyst score is based on the extent of focal bone loss through individual cysts (illustrated in central region) or multiple cysts (illustrated in posterior region) along the articular surface.

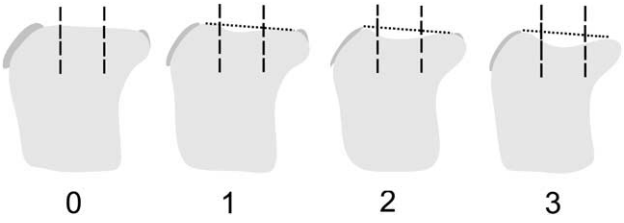

Fig. 6. Subarticular bone attrition score. Bone attrition is scored on the basis of the degree of flattening or depression of the articular surface relative to normal.

The maximum scores for MFTJ, LFTJ, PFJ, region S and the entire knee were 15, 15, 12, 3 and 45 respectively (Table I).

Flattening or depression of the articular surfaces was termed bone attrition and graded from 0 to 3 based on the subjective degree of deviation from the normal contour: 0=normal; 1=mild; 2=moderate; 3=severe. For example, the osseous articular surfaces of the medial and lateral femoral condyles and medial facet of the patella are all normally slightly convex. Accordingly, flattening=Grade 1, slight concavity=Grade 2, and marked concavity=Grade 3. Fig. 6 illustrates this for the lateral tibial plateau (Fig. 6). The maximum scores for the MFTJ, LFTJ, PFJ and the entire knee were 15, 15, 12 and 42 respectively (Table I).

Osteophytes along 14 different margins of the knee, the anterior (*a*), central weight bearing (*c*) and posterior (*p*) margins of the femoral condyles and tibial plateaus, and the medial (M) and lateral (L) margins of the patella, were graded from 0 to 7 using the following scale: 0=none; 1=equivocal; 2=small; 3=small-moderate; 4=moderate; 5=moderate-large; 6=large; 7=very large (Figs. 7 and 8). The maximum scores for the MFTJ, LFTJ, PFJ and the entire knee were 35, 35, 28, and 98 respectively (Table I).

The anterior cruciate ligament (ACL) and posterior cruciate ligament (PCL) were independently scored as intact (0) or torn (1) using the sagittal T2 FSE images. The medial collateral ligament (MCL) and lateral collateral ligament (LCL) were independently scored as intact (0), or torn (1)

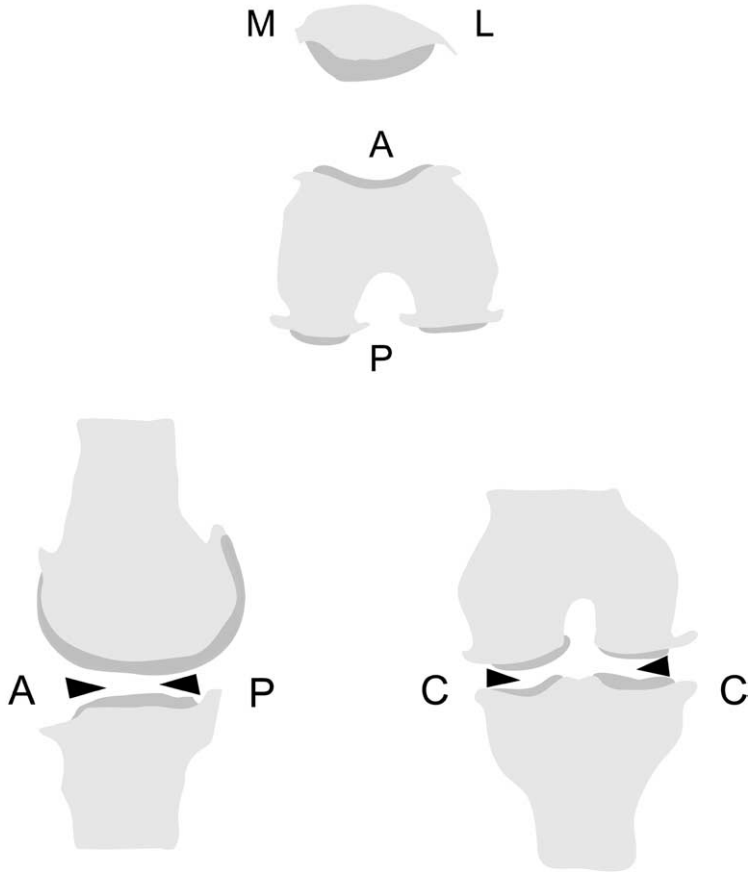

Fig. 7. Regional subdivision of the articular margins. A. Patellar medial (M) and lateral (L) margins are evaluated using axial images. B. Femorotibial anterior (A) and posterior (P) margins are evaluated by combining information from both axial and sagittal (left panel) planes, whereas the central (C) femorotibial margins are evaluated using the coronal images (right panel).

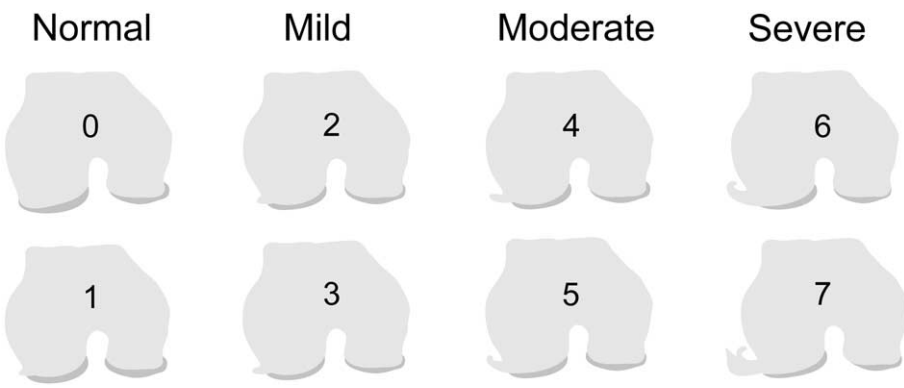

Fig. 8. Eight-point scale for scoring marginal osteophytes. Osteophytes are scored on an eight-point scale based on size and the extent of margin involvement by the bone spur.

Table II
Scheme for determining total scores for the medial and lateral meniscus

Score	Grades*
0	All 0
1	At least one 1, but no >1
2	2 in only one region
3	2 in more than one region
4	3 in one or more region
5	4 in only one region
6	4 in more than one region

*Regions: Ant, Body, Post

using the coronal images. A combined ligament score was calculated by adding the sum of the ACL and PCL scores to half the sum of the MCL and LCL scores.

The anterior horn, body segment and posterior horn of the medial and lateral menisci were graded separately from 0 to 4 based on both the sagittal and coronal images: 0=intact; 1=minor radial tear or parrot-beak tear; 2=non-displaced tear or prior surgical repair; 3=displaced tear or partial resection; 4=complete maceration/destruction or complete resection. A cumulative grade for each meniscus was also determined using the scheme shown in Table II. This algorithm was needed in order to adjust for non-linearity among the regional grades, which could lead to inconsistencies if the grades were simply summed. For example, if a meniscus had a grade-2 tear in the body and posterior horn, simply summing these regional grades would yield the same total score (4) as for a meniscus that was completely missing its posterior horn, even though the latter abnormality would be a far greater biomechanical insult to the knee. The corresponding scores derived with the conversion algorithm, however, would be 3 and 5, respectively.

Synovial thickening and joint effusion were not distinguished from each other, but graded collectively from 0 to 3 in terms of the estimated maximal distention of the synovial cavity: 0=normal; 1=<33% of maximum potential distention; 2=33%–66% of maximum potential distention; 3=>66% of maximum potential distention.

Loose bodies in the synovial cavity were scored from 0 to 3 based on number: 0=none; 1=1 loose body; 2=2 loose bodies; 3=3 or more loose bodies.

Synovial cysts or bursal collections about the knee were specified (e.g., popliteal, anserine, semimembranosis, meniscal, infrapatellar, prepatellar, tibiofibular, etc.) and graded 1 to 3 based subjectively on size.

Any other findings (e.g., patellar tendon or quadriceps tendon abnormalities, avascular necrosis, stress fracture, insufficiency fracture, focal osteochondral fracture, bone or soft-tissue tumors) were specified.

Technical limitations, such as failed fat suppression or metallic artifacts that interfered with the reliability of the scoring of a particular case were noted.

The final WORMS scores were tabulated as (1) independent values for each feature in each of the three compartments of the knee (PFJ, MFTJ and LFTJ), (2) cumulative surface feature (cartilage, marrow abnormality, subarticular cysts, bone attrition, osteophytes) scores for each compartment, (3) cumulative scores for each feature throughout the knee, and (4) a total combined score for the entire knee.

STATISTICAL ANALYSES

Scores were summarized as means and standard deviations (SD), Inter-observer agreement was based on the exact rating of each feature, not just the presence or absence of each feature, and expressed as intraclass correlation coefficients (ICC) by treating the data as continuous variables. The ICC was used because it combines a measure of correlation with a test of the difference of means and is therefore a more appropriate test than Pearson's correlation coefficient, which does not take into account bias between readers[6]. Associations among features were expressed as Spearman's Rho.

Results

Table III shows the frequency of involvement (score >0) of each feature in the study population. Each compartment showed abnormalities more than 90% of the time. Ninety-eight percent of knees showed cartilage abnormalities. This was most frequent (94%) in the PFJ, but involvement of the MFTJ and LFTJ was also very common (89% and 71%, respectively). Ninety-two percent of knees showed osteophytes. The compartmental prevalence was approximately 80%. Fifty-seven percent of knees showed bone marrow abnormality, most commonly in the MFTJ (35%). Bone cysts were present in 77% of knees, most commonly in the PFJ (38%), and bone attrition was present 48% of the time, most commonly in the MFTJ (29%). Eighty percent of the

Table III
Percent involvement

	MFTJ	LFTJ	PFJ	S Region	Total
Cartilage	89%	71%	94%		98%
Marrow abnormality	35%	17%	16%	14%	57%
Bone cysts	34%	18%	38%	38%	77%
Bone attrition	29%	13%	17%		48%
Osteophytes	83%	79%	81%		92%
Compartment total	94%	97%	91%		
Menisci	70%	36%			80%
Ligaments					8%
Synovitis					75%
Total					100%

Table V
Mean score as a percent of maximum possible score

	MFTJ	LFTJ	PFJ	S Region	Total
Cartilage	50%	27%	46%		39%
Marrow abnormality	7%	3%	3%	7%	4%
Bone cysts	7%	3%	7%	17%	7%
Bone attrition	4%	2%	3%		2%
Osteophytes	26%	9%	21%		21%
Compartment total	24%	14%	20%		–
Menisci	50%	17%			33%
Ligaments					3%
Synovitis					33%
Total			–		18%

knees showed meniscal abnormalities. Abnormalities were almost twice as common in the medial meniscus (70%) as they were in the lateral meniscus (36%). Two patients had lateral meniscal cysts (grades 2 and 3). Synovial distention was present in three-quarters of the patients, but ligament abnormalities were seen in only 8%. Eleven subjects had popliteal cysts. Four of these were grade 1, five were grade 2, and two were grade 3 dissecting cysts. Two subjects had cysts of the proximal tibiofibular joint (grades 1 and 2). One of these also had a grade-3 popliteal cyst. One patient had grade-1 prepatellar bursitis. No cases of anserine bursitis were identified. No intra-articular loose bodies were identified.

Table IV shows the mean scores and their standard deviations for each feature (not including bursae and cysts) in the study population. As indicated in Table V most of these scores were in the lower quarter of their possible range. MFTJ cartilage score (50%) and medial meniscal score (50%) were the highest in this regard, where as bone marrow abnormality (4%), bone cysts (7%), bone attrition (2%) and ligament (3%) scores were in the lower tenth of their respective severity ranges.

Table VI shows the agreement (ICC) between the two readers in this study. All values were greater than 0.61, and most were greater than 0.80. ICCs for cartilage and osteophyte scores were greater than 0.9. The poorest agreement was for bone attrition, but the prevalence of this feature was extremely low, particularly in the PFJ and LFTJ where the frequency of positive scores was too low to calculate ICC reliably.

As shown in Table VII, scores among many of the individual features, particularly cartilage, bone cysts, bone attrition, osteophyte and meniscus, were relatively strongly associated. Interestingly, meniscal scores associated strongly with ipsilateral FTJ scores but poorly with contralateral FTJ score or with PFJ scores (Tables VII and VIII). Associations between features in region S (marrow abnormality and bone cysts) and those elsewhere in the knee were poor.

Discussion

MRI offers a unique opportunity to evaluate all components of a joint simultaneously and therefore to provide a whole organ assessment of the status of structural damage in patients with OA. Whole-organ assessment could help discriminate different patterns of intra-articular involvement in OA; detect early, potentially preclinical, stages of OA; identify structural risk factors for developing clinical OA; or increase scope and sensitivity to change for monitoring disease progression and treatment response in patients with established OA. This would aid subject selection, treatment monitoring, and safety assessment in clinical trials of putative new therapies for OA and in studies exploring the pathophysiology and epidemiology of OA.

The semiquantitative whole-organ MRI scoring (WORMS) method presented in this report offers an initial instrument for performing multi-feature assessment of the knee using conventional MRI. It takes into account a variety of features that are currently believed to be relevant to the functional integrity of the knee and/or potentially involved in the pathophysiology of OA. It scores each of these features with a sufficient number of increments to allow detection of what are speculated to be clinically relevant changes – although, this was not explicitly tested in the current cross

Table IV
*Mean scores**

	MFTJ	LFTJ	PFJ	S Region	Total
Cartilage	15 (9)	8 (9)	11 (6)		33 (17)
Marrow abnormality	1 (0.9)	0.4 (1)	0.4 (1)	0.2 (0.6)	2 (3)
Bone cysts	1 (2)	0.4 (1)	0.8 (1)	0.5 (0.7)	3 (3)
Bone attrition	0.6 (1)	0.3 (0.9)	0.3 (0.8)		1 (2)
Osteophytes	9 (7)	6 (6)	6 (5)		21 (16)
Compartment total	26 (18)	15 (15)	18 (10)		
Menisci	3 (2)	1 (2)			4 (3)
Ligaments					0.1 (0.3)
Synovitis					1 (1)
Total					60 (33)

*Values are mean score (standard deviation) for each feature

Table VI
Inter-reader agreement (ICC)

	MFTJ	LFTJ	PFJ	S Region	Total
Cartilage	0.98	0.99	0.98		0.99
Marrow abnormality	0.90	0.96	0.82	1.0	0.74
Bone cysts	0.98	0.95	0.73	1.0	0.94
Bone attrition*	0.61	–	0.78		–
Osteophytes	0.93	0.94	0.98		0.97
Compartment total	0.97	0.98	0.99		
Menisci	0.94	0.81			0.87
Ligaments					1.0
Synovitis					0.74
Total					0.98

*The frequency of cases of bone attrition in the LFTJ was too small to reliably calculate ICC.$P<0.01$ for all other values.

Table VII
Spearman Rho for association between cartilage scores and the corresponding comparmental and total scores of other features

	MFTJ	LFTJ	PFJ	Total
Marrow abnormality	0.73*	0.43	0.40	0.21
Bone cysts	0.61*	0.57*	0.62*	0.49*
Bone attrition	0.56*	0.11	0.60*	0.37
Osteophytes	0.81*	0.47*	0.51*	0.66*
Medial meniscus	0.75*	0.08	–0.16	0.50*
Lateral meniscus	0.08	0.47*	0.21	0.50*
Ligament	–0.17	0.18	0.00	0.00
Synovitis	0.40	–0.34	0.25	0.21

*Prob>|Rho| was 0.05 or less.

Table VIII
Spearman Rho among meniscal and compartment-total scores.

	Meniscus	
Total	Medial	Lateral
MFTJ	0.80*	0.07
LFTJ	–0.04	0.55*
PFJ	–0.02	0.05

*$P<0.01$.

sectional study design. Based on the conditions of this study, it shows high inter-reader agreement among trained radiologists experienced in MRI interpretation of the knee, and employs conventional MR images that can be produced with clinical MRI systems available at most hospitals and imaging centers around the world. It must be emphasized, however, that WORMS and its constituent subscores are not claimed to be the definitive instrument for whole-organ MRI evaluation of the knee, but rather a first step in what is hoped will be a process of continuous improvement and refinement of the basic scheme.

WORMS incorporates 14 articular features. Of these, articular cartilage loss and osteophytes are the most broadly accepted as being central to the pathophysiology of OA. MRI is ideally suited to imaging these two cardinal features. Cartilage imaging with MRI, in particular, has received considerable attention in the past several years.

Numerous studies have shown MRI to be highly sensitive and specific for detecting focal cartilage defects and thinning[7–11]. The most commonly used pulse sequences for examining articular cartilage have been fat-suppressed, T1-weighted, 3D gradient-echo[7] (Fig. 9) and fat-suppressed T2-weighted or intermediate-weighted FSE[9–11] (Figs. 10–12). Both of these techniques are easy to perform and widely available on conventional clinical MRI systems. In this study we combined information from both techniques to evaluate the cartilage. Several investigators have developed and validated computer-assisted methods for quantifying articular cartilage volume and thickness[12–16,18,20]. WORMS, however, relies on semiquantitative assessment by the trained eye.

A number of semiquantitative scoring methods for grading cartilage loss on MRI have been developed[19,21–23], but no single method has been accepted broadly as a standard for clinical research thus far. Most of these scoring strategies derive from arthroscopy, and grade primarily the depth of focal cartilage loss over a four-point scale. The method employed in WORMS is also based on this classic scheme, but expands the scale to eight points in order to capture different patterns of regional cartilage loss and more information about extent of surface involvement (Fig. 3). Each point on the scale is one integer, except for grade 2.5. This point interval is smaller than the others are because the difference in cartilage loss between a small focal partial-thickness defect (2.0) and a small focal full-thickness defect (2.5) is proportionately smaller than the difference between the other intervals. The adjustment, accordingly, improves linearity of the scale. WORMS also incorporates changes in cartilage signal on T2-weighted images, which have been shown to represent areas of chondromalacia that may precede focal tissue loss[24–27]. Despite the expanded scale of the WORMS cartilage score, inter-reader reproducibility was high (Table VI). The longitudinal reproducibility of this method was not addressed in this cross sectional study design, but the extra increments in the scale would be expected to increase sensitivity to change. Exactly how much change is clinically relevant is not currently known. However, in the population of OA patients examined in this study, most knees fell into the midrange of possible scores for cartilage damage (Table V). One consequence of using a larger scale for cartilage than for other features – besides osteophytes – is that cartilage score is given greater weight in the total score for the knee. This may be appropriate, given the importance that articular cartilage is believed have in the pathophysiology of OA. However, this requires validation in longitudinal studies.

Cartilage score was determined independently in each of 14 articular surface regions. The femoral surface was divided into anterior, central and posterior regions based on the different relative functions of these regions (Fig. 1). The tibial surface was similarly subdivided into anterior, central and posterior regions in order to allow examination of associations with abnormalities of the anterior horn, body and posterior horn of the meniscus, respectively. The anterior and posterior osteochondral junctions and the insertions of the meniscal ligaments to the joint capsule were used as the anatomical landmarks for subdividing the articular surface. This was because these landmarks were easily identified on most MRI examinations and because they delimited surfaces of relatively different function within the knee. The anterior region of the femoral cartilage corresponded to the patellofemoral joint, the central region between the anterior and posterior meniscal ligaments corresponded to the area of the femoral cartilage loaded during standing and normal walking, and the posterior region corresponded to the area loaded during deep flexion of the knee. It was felt that this subdivision strategy yielded

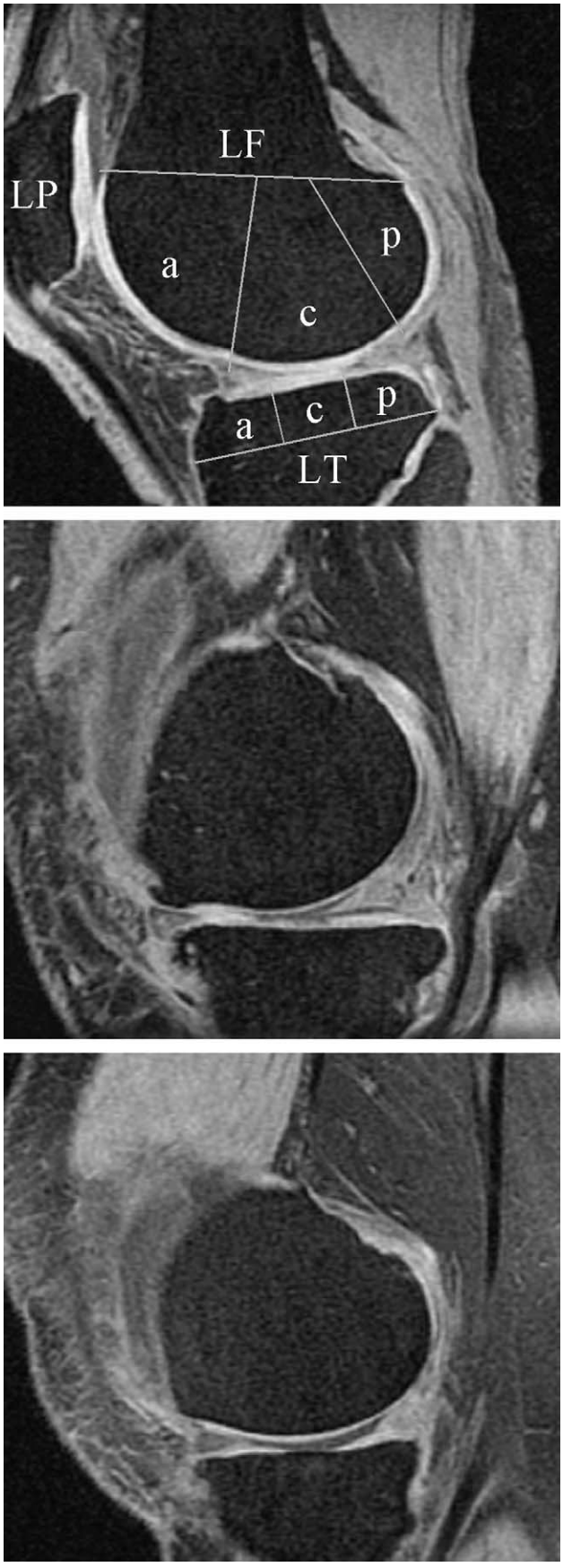

the optimal compromise between reproducibility and functional correlation. It should be noted that each reader subdivided the joints independently. Accordingly, this potential source of variability was included in the assessments of inter-observer reproducibility (Table VI). How this may be affected by meniscal subluxation or tear, or by longitudinal study designs was not, however, addressed.

The imaging protocol used in this study was designed for whole organ assessment rather than optimal evaluation of any individual feature, and accordingly it embodied a number of compromises to that end. Alternative techniques could have yielded better assessments of certain structures in more focused protocols. With respect to cartilage imaging, for example, the spatial resolution of the MR images used in this study were only 547 μ×729 μ×4000 μ for T2-weighted FSE and 547 μ×2000 μ for FS-3DSPGR. Higher-resolution pulse sequences may have shown greater sensitivity for small focal cartilage defects and mild cartilage thinning, and may also have yielded greater reader reproducibility, albeit at the cost of longer imaging time. A number of other modifications to the imaging protocol may also have improved cartilage assessment. For example, acquiring FSE or FS-3DSPGR images in the axial plane in addition to the sagittal plane used in this study could have improved assessment of the patellar cartilage. Also, shortening the TE of the FSE sequence would have increased contrast between articular cartilage and subchondral bone, and may have thus improved cartilage thickness assessment on those images. However, FS-3DSPGR is better than FSE for assessing cartilage thickness, and it is possible that shorter-TE FSE sequences are less specific for cartilage signal abnormality than longer TE-FSE sequences are.

Osteophytes are also well delineated with MRI (Figs. 9–13). In fact, because of its tomographic viewing perspective MRI can delineate osteophytes more reproducibly than radiography can, and detect osteophytes in locations that would otherwise be obscured by projectional superimposition on conventional radiographs[5,28]. The WORMS osteophyte score was based on the method used in the Osteoarthritis Research Society International (OARSI) Atlas for radiographic assessment of osteophytes in the knee[29]. In contrast to the four-point OARSI score, however, the WORMS score used an expanded eight-point scale. As for the WORMS cartilage score, increasing the number of increments conferred greater sensitivity to change, but still

Fig. 9. Sagittal fat-suppressed T1-weighted 3D gradient-echo. A. White lines demarcate the anterior (a), central (c) and posterior (p) subdivisions of the lateral femoral condyle (LF) and lateral tibial plateau (LT). This image shows grade 3 cartilage loss over the LFc and LFp regions, and grade 4 cartilage loss over the LTp region. The cartilage over the LTc and anterior portions of the LFc, however, shows normal thickness. Accordingly, conventional extended-knee radiography, which samples only these two cartilage regions would be expected to show normal joint-space width in this knee despite the cartilage loss evident with MRI more posteriorly along the LFc. B. Grade 4 cartilage loss over the MTc, and Grade 5 loss over the MFc and MFp. Image C shows grade 6 cartilage loss over MTc, grade 4 loss over MFc and grade 5 loss over MFp. Note also the osteophytes delineated in images A (grade 2 LTa), B (grade 3 MFa, grade 4 MFp, grade 3 MTa, grade 4 MTp) and C (grade 2 MTa, grade 2 MTp). This image also shows synovial distension and a small popliteal cyst, but the contrast properties of this pulse sequence are not ideal for this. It is important to emphasize that multiple image sections, not just single images as in these examples, must be examined in order to score even individual subdivisions of the knee properly

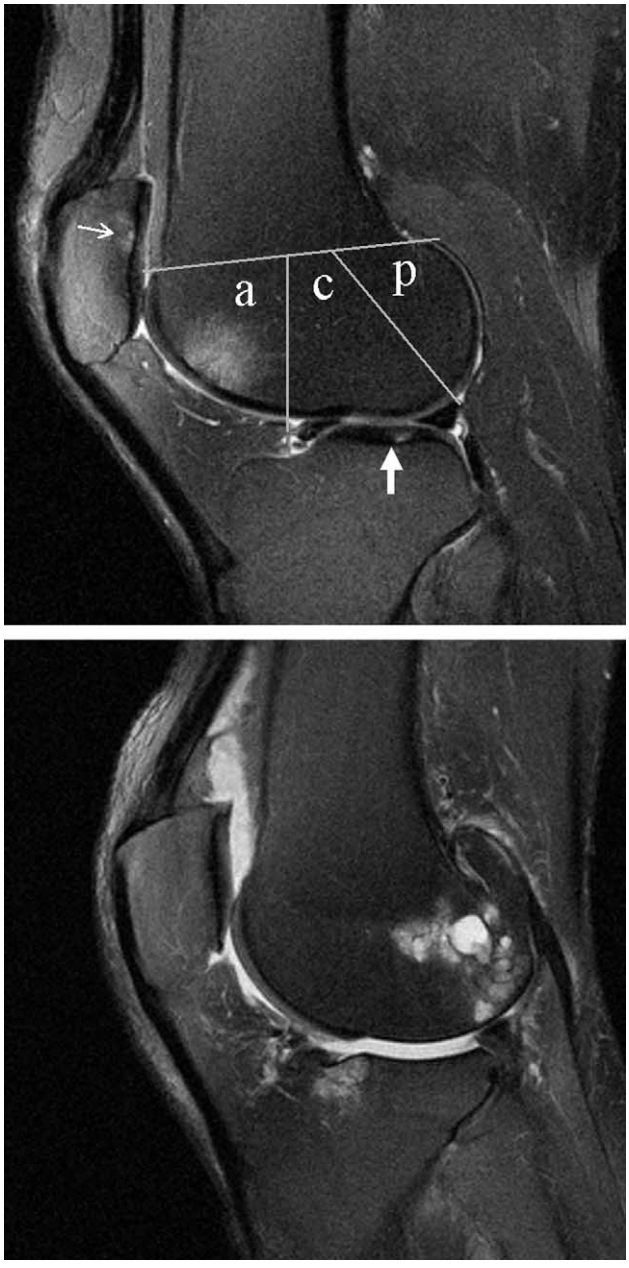

Fig. 10. Sagittal T2-weighted FSE. A. Focal grade 1 cartilage signal lesion (large arrow) is present in the LTc region, grade 3 cartilage loss over the LFp and LP, and grade 3 marrow abnormality in the LFa. Grade 1 subarticular cyst (small arrow) is noted beneath the thinned cartilage of the LP. This image also shows mild failure of fat suppression over the patella. This artifact occasionally arises in this location because the irregular shape of the patella perturbs the local magnetic field and alters the resonant frequency of fat, upon which frequency-selective fat suppression is based. Fat-suppression failure could easily be mistaken for marrow abnormality, except that the latter respects osseous boundaries, whereas frequency shifts often extend into the surrounding soft tissues. B. A milder example of this phenomenon is also seen in this image. Other findings include grade 3 subarticular cysts in LFp; complete denuding (grade 6) of articular cartilage over LFc, LFp and all three regions of LT; grade 3 marrow abnormality in LTa; grade 1 bone attrition across LT; grade 2 and grade 7 osteophytes of LTa and LFp, respectfully; and grade 4 destruction of the anterior horn of the lateral meniscus.

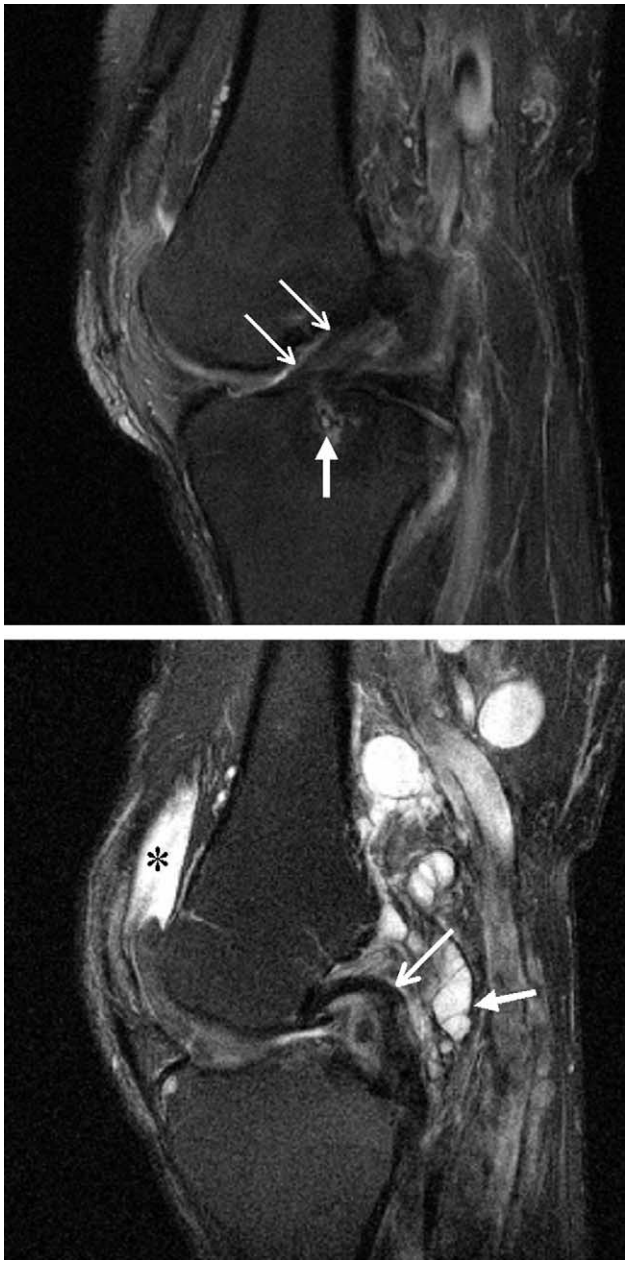

Fig. 11. Imaging the ACL. A. Midsagittal fat-suppressed T2-weighted FSE image shows an intact (grade 0) ACL (small arrows). Note the small cyst (large arrow) at the tibial insertion of the ACL in region S. B. The same image of another knee shows complete absence of the ACL, indicative of tear (grade 1). Anterior subluxation of the tibia and bowing of the PCL (small arrow) are additional features directly associated with ACL tear. A joint effusion (*) and popliteal cyst (large arrow) are also present.

provided high inter-reader reproducibility (Table VI). Also like cartilage score, the extra increments in this scale gave osteophyte score greater weight in the total score. While 92% of knees included in this study had osteophytes, most fell into the lower quarter of the severity range of the WORMS osteophyte score.

Subarticular bone cysts and bone attrition are also characteristic, albeit late, features of OA that are well delineated with conventional MRI (Fig. 10). The WORMS

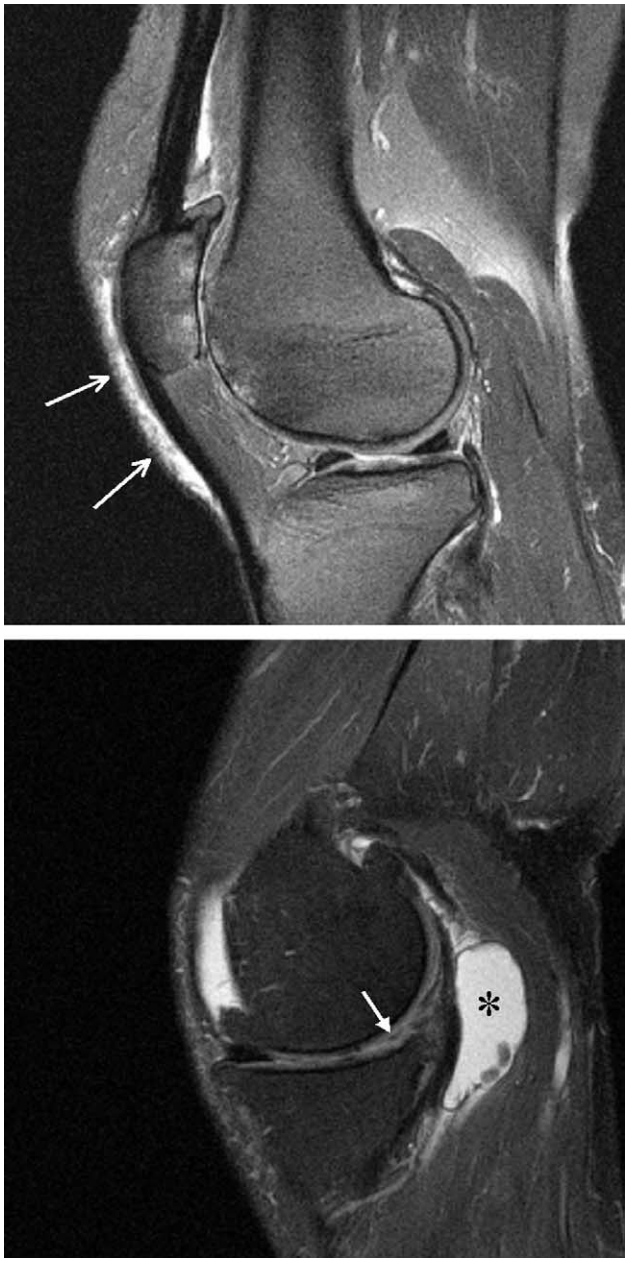

Fig. 12. Periarticular bursitis and cysts. A. Fluid signal over the patellar tendon (arrows) on this sagittal fat-suppressed T2-weighted image represents prepatellar bursitis. The robustness of fat suppression in the adjacent soft tissues argues against failed fat suppression as an explanation (see Fig. 10). Additional findings on this image include grade 3 cartilage loss over the LTc, grade 5 cartilage loss over the LFa, grade 6 cartilage loss over the LP, grade 1 subarticular cysts of the LFa, and grade 2 subarticular abnormality of the LP. B. Sagittal T2-weighted FSE images through the medial TFJ shows a grade 2 popliteal cyst (*). Image B also shows grade 4 osteophytes of MFa, MFp, and MTa, a grade 2 osteophyte of MTp, and grade 4 destruction of the posterior horn of the medial meniscus (arrow).

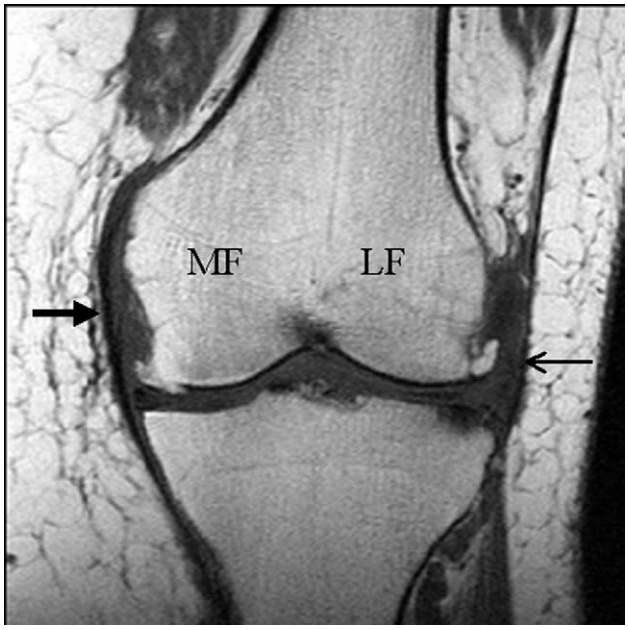

Fig. 13. Coronal T1-weighted spin echo. This image shows grade 3 osteophytes of MFc and LFc, and a grade 2 osteophyte of LTc with adjacent subarticular marrow abnormality. Additionally, the lateral meniscus shows a bucket-handle tear (grade 3) of the body region. The MCL (large arrow) and illiotibial band (small arrow), which is a portion of the LCL, are intact. Articular cartilage is not delineated with T1-weighted spin-echo images.

bone cyst score employs a simple four-point scale based on the extent of regional involvement by individual cysts or multiple cysts along the articular surface. Because of its tomographic viewing perspective, MRI would be expected to be more sensitive than projectional radiography for detecting subarticular cysts, much as has been shown to be the case for bone erosions in rheumatoid arthritis[30–34]. The WORMS bone attrition score employs a four-point scale based on the subjective degree of flattening or depression of the articular cortex relative to normal, analogous to the radiographic attrition score outlined in the OARSI Atlas[29]. In contrast to the cartilage score and the osteophyte score, the scales of the bone attrition score and the bone cyst score were not expanded beyond four-points, because it was felt that doing so would result in greater reproducibility error and therefore would not provide additional sensitivity to change. We did not, however, formally test this assumption.

In addition to the features described above, areas of abnormal MRI signal have been observed in the subarticular marrow of osteoarthritic knees[3,35,36]. Because of the resemblance of this feature to changes commonly seen in trauma, infection, inflammation and acute ischemic necrosis[37], it has often been referred to as ‘marrow edema’. However, histological correlations with MR images of specimens acquired from total knee replacement surgery showed that edema per se was not actually a prevalent constituent of this MRI feature[38]. Accordingly, the more general term ‘marrow abnormality’ is used in this report. Regardless, the presence of this finding in OA is strongly associated with pain, especially when cartilage loss is severe. In a study of 401 patients with knee OA, Felson, *et al.*[3] reported that 78% (272) of those with pain (351) compared to only 30% (15) of those without pain (50) showed this marrow abnormality on MRI. Moreover, large marrow lesions were seen almost exclusively in patients with knee pain (36% vs 2%). More recently, Felson reported that these changes were highly predictive of subsequent ipsilateral cartilage loss in the knee, and that

their presence identified most knees at risk for progression[36]. Whether this feature in OA reflects microtrauma due to biomechanical incompetence of the articular surface, and whether interventions that decrease its extent also diminish pain and structural progression are not known. However, in contrast to some other features of OA, such as cartilage loss, bone marrow abnormality has been observed to change quite rapidly-sometimes in a matter of only months[39]. Because of the responsiveness of this feature in comparison to other findings associated with OA, its relationship to other structural abnormalities in the knee and its potential role in the pathophysiology of OA are key issues to be addressed.

Marrow abnormalities are most sensitively demonstrated with fat-suppressed T2-weighted spin-echo or fast spin echo images and short-tau inversion-recovery (STIR) images. In this study we used the former. One limitation of fat-suppressed T2-weighted images is that local magnetic field heterogeneities near irregularly shaped anatomy, such as the patella, or near metal can result in areas of failed fat suppression, which can mimic marrow abnormality. Marrow abnormality can also be seen on heavily T1-weighted images but not as sensitively as with fat-suppressed T2-weighted images. Marrow abnormality was seen in just over half of the knees included in this study (Table III), and the majority of the lesions were moderate (grade 2) (Tables III and IV).

Other structures evaluated in WORMS include the menisci. For over a decade, MRI has been the method of choice for evaluating meniscal pathology, but it has only been in the last several years that the relationship between this articular structure and other tissues in the knee, particularly with respect to the pathophysiology of OA, has gained significant attention. A number of studies have shown that meniscectomy leads to articular cartilage loss and knee OA and is associated with long-term symptoms and functional limitation[17,40,41]. Studies have also shown that meniscal subluxation can be an independent cause of radiographic joint-space narrowing[42–44]. One study by Kawahara, *et al.*[45] reported that abnormal movement of the meniscus on dynamic MRI correlated with the severity of cartilage damage in the knee. The meniscal score used in WORMS is based on surgically and histologically validated MRI grading schemes that have been used in clinical practice for more than a decade[46]. In addition to grading degenerative and traumatic meniscal damage progressively from small radial tears of the free margin to displaced bucket-handle tears and maceration of the horns and body, WORMS accounts for surgical changes, such as repair, partial resection and complete resection. The current version of WORMS does not, however, account for subluxation of the menisci.

Meniscal tears are most sensitively delineated with short-TE MRI pulse sequences, such as T1-weighted spin echo (Fig. 13), proton density weighted spin echo and T2*-weighted gradient echo[46]. The majority of meniscal tears are demonstrable on sagittal images, but a small percentage of body-segment tears are visible only on coronal images. Accordingly, both planes were used in this assessment.

Ligamentous insufficiency is believed to be another important driver of meniscal tear, cartilage loss and OA[47,48]. MRI has long been the method of choice for assessing the cruciate and collateral ligaments of the knee[49]. Ligaments and tendons are best examined with long-TE MRI techniques because so called 'magic-angle' effects[50] on short-TE images can mimic inflammation and tear. Indeed, the magic-angle phenomenon must be considered in all collagen-containing structures, including articular cartilage[51] and the menisci[52]. The ACL and PCL are typically assessed in the sagittal plane (Fig. 11), whereas the MCL and LCL are assessed in the coronal plane (Fig. 13). In this study, ligament integrity was scored on a binary scale as intact (0) or torn (1) based on established MRI criteria[49]. Occasionally, remote complete tears or chronic repetitive partial tears can heal with residual laxity while appearing intact or thickened on MRI[49]. These variants of ligament damage were not accounted for in the current WORMS score. A total ligament score for the knee was calculated by combining the individual scores for ACL, PCL, MCL and LCL, and applying a weighting factor of 0.5 to the collateral ligament scores in order to account for the greater importance of cruciate ligament damage to functional impairment of the knee.

MRI is also useful for assessing synovitis and joint effusions. Some degree of synovial thickening can be found in a majority of osteoarthritic joints[53]. Whether this synovitis contributes directly to articular cartilage loss in OA, or simply arises in reaction to the breakdown of cartilage by other causes remains a controversy[54]. However, synovitis may be important to the symptoms and disability of OA, and pose different treatment requirements than simple 'chondroprotection'. The WORMS system described in this report scores synovitis in terms of distension of the synovial cavity, without distinguishing between synovial tissue and synovial fluid. MRI is capable of differentiating between these components, but this requires the use of special techniques, such as magnetization-transfer subtraction[55], fat-suppressed, T1-weighted imaging[55], or intravenous injection of gadolinium (Gd)-containing contrast material[55–58]. By monitoring the rate of synovial enhancement with Gd-containing contrast over time using rapid, sequential MRI, it is furthermore possible to grade the severity of the synovitis in these patients. The majority of work in this area has, however, focused on rheumatoid arthritis thus far, and experience with OA is limited. It is also possible to quantify the volume of synovial fluid or synovial tissue in the knee, to the extent that these two components are discriminated from each other with the imaging protocol used[59]. Intravenous Gd-containing contrast media can be used for this; however, diffusion of contrast material from synovial tissue into adjacent synovial fluid rapidly obscures the boundary between these two components, and complicates the practical applicability of this approach[55]. Accordingly, the present WORMS system did not attempt to differentiate synovial tissue from synovial effusion, but rather combined them into a single score based on conventional fat-suppressed, T2-weighted fast spine echo images. Seventy-five percent of the knees in this study showed some synovial distension (Table III), but in most cases the degree was mild (Table IV).

Finally, periarticular bursitis and cysts can be causes of pain and dysfunction in the knee that mimic or contribute to the clinical presentation of OA[35,60,61]. The most common of these are popliteal cysts, which communicate with the synovial cavity through a space between the tendons of the semimembranosis and medial gastocnemius muscles. Most popliteal cysts are small and clinically occult, but some grow to several hundred ml and can produce posterior swelling and interfere with knee flexion. Occasionally, these cysts rupture causing local inflammation and acute calf pain. Fifty-eight percent (11) of the patients in this study had popliteal cysts, but only two of these were grade

3, and none were ruptured. Cysts of the proximal tibiofibular joint, anserine bursitis, semimembranosis bursitis and prepatellar bursitis are additional potential causes of pain and swelling about the knee that are sensitively identified and easily discriminated from one and other with MRI. Two cases of tibiofibular cysts and one case of prepatellar bursitis were noted in the patients included in this study.

Table IV presents a number of features in WORMS in a matrix of individual and cumulative scores across and within the various compartments of the knee. The multifeature, multi-regional nature of WORMS provides a richer picture of structural changes in the knee than has been available thus far with noninvasive methods, and promises to provide new insights into the causes and possible therapies of this enigmatic disease. In the group of patients examined in this study, the cumulative score for articular surface features in the PFJ associated at least mildly with those in the MFTJ and LFTJ, whereas the cumulative scores for MFTJ and LFTJ associated only poorly with each other. Part of the reason for this may be the fact that the femorotibial compartments of the knee are physically connected to each other, so that narrowing in one due to cartilage loss and/or meniscal subluxation will result in widening and decreased mechanical loading in the other. Accordingly, progressive damage in one TFJ may actually have a protective effect on the other TFJ.

Meniscal score associated strongly with the cumulative surface-feature score of the ipsilateral FTJ but not with that of the contralateral FTJ or the PFJ (Table VIII). This suggests that damage to the meniscus is either a cause of ipsilateral structural damage or is itself caused by damage to these local structures. The cross sectional design of the current study, however, does not allow discrimination of these alternatives. The strongest associations among the WORMS features were for cartilage, osteophyte and meniscal scores (Tables VII and VIII). Such interassociations are consistent with an organ-failure model of OA pathophysiology. How these structural changes relate to each other, however, and how predictive each is of changes to other structures in the knee are not currently known, but these questions are being addressed in ongoing epidemiological studies and initiatives, such as the NIH OA Initiative (http://www.niams.nih.gov/ne/oai/index.htm), and hopefully will be answered in the future.

In conclusion, WORMS represents an initial semiquantitative scoring system for whole-organ assessment of the knee in OA using MRI. While this approach is still in its infancy, it provides a more comprehensive picture of structural changes in OA than previous methods do, and it offers high inter-reader agreement, at least among radiologists experienced with the technique. Moreover, WORMS employs conventional MR images that can be produced with clinical MRI systems available at most hospitals and imaging centers around the world. Further validation and refinement of WORMS is still needed in order to maximize its utility in clinical trials and epidemiological studies. The version presented in this report, therefore, is not intended as a definitive solution but rather an initial step in what is hoped to be a continuous process of development and improvement in whole-organ evaluation of joints with OA.

Acknowledgements

Support for this study was provided in part by Bayer Corp., the National Institutes of Health and Synarc, Inc.

References

1. Hochberg MC, Lawrence RC, Everett DF, Cornoni-Huntley J. Epidemiologic associations of pain in osteoarthritis of the knee: data from the National Health and Nutrition Examination Survey and National Health and Nutrition Examination-I Epidemiologic Follow-up Survey. Semin Arthritis Rheum 1989;18:4–9.
2. Summers M, Haley W, Reveille J, Alarcón G. Radiographic assessment and psychologic variables as predictors of pain and functional impairment in osteoarthritis of the knee or hip. Arthritis Rheum 1988; 31:204–9.
3. Felson DT, Chaisson CE, Hill CL, *et al.* The association of bone marrow lesions with pain in knee osteoarthritis. Ann Intern Med 2001;134:541–9.
4. Hirasawa Y, Okajima S, Ohta M, Tokioka T. Nerve distribution to the human knee joint: anatomical and immunohistochemical study. Int Orthop 2000;24:1–4.
5. Peterfy C. Imaging Techniques. In: Klippel J, Dieppe P, Eds. Rheumatology 2E. Philadelphia: Mosby 1998; 1:14.1–14.18.
6. Kramer M, Feinstein A. Clinical biostatistics LIV; the biostatistics of concordance. Clin Pharmacol Ther 1981;29:111–23.
7. Recht MP, Pirraino DW, Paletta GA, Schils JP, Belhobek GH. Accuracy of fat-suppressed three-dimensionl spoiled gradient-echo FLASH MR imaging in the detection of patellofemoral articular cartilage abnormalities. Radiology 1996;198:209–12.
8. Disler D. Fat-suppressed three-dimensional spoiled gradient-recalled MR imaging: assessment of articular and physeal hyaline cartilage. AJR 1997;169: 1117–23.
9. Bredella M, Tirman P, Peterfy C, *et al.* Accuracy of T2-weighted fast spin-echo MR imaging with fat saturation in detecting cartilage defects in the knee: comparison with arthroscopy in 130 patients. Am J Roentgenol 1999;172:1073–80.
10. Broderick L, Turner D, Renfrew D, Schnitzer T, Huff J, Harris C. Severity of articular cartilage abnormality in patients with osteoarthritis: evaluation with fast spin-echo MR vs arthroscopy. Am J Roentgenol 1994; 162:99–103.
11. Kawahara Y, Uetani M, Nakahara N, Doiguchi Y, Nishiguchi M, Futagawa S. Fast spin-echo MR of the articular cartilage in the osteoarthrotic knee. Correlation of MR and arthroscopic findings. Acta Radiol 1989;39:120–5.
12. Peterfy CG, van Dijke CF, Janzen DL, *et al.* Quantification of articular cartilage in the knee by pulsed saturation transfer and fat-suppressed MRI: optimization and validation. Radiology 1994;192:485–91.
13. Pilch L, Stewart C, Gordon D, *et al.* Assessment of cartilage volume in the femorotibial joint with magnetic resonance imaging and 3D computer reconstruction. J Rheum 1994;21:2307–21.
14. Eckstein F, Sitteck H, Gavazzenia A, Milz S, Putz R, Reiser M. Assessment of articular cartilage volume and thickness with magnetic resonance imaging (MRI). Trans Orthop Res Soc 1995;20:194.
15. Eckstein F, Winzheimer M, Hohe J, Englmeier KH, Reiser M. Interindividual variability and correlation among morphological parameters of knee joint cartilage plates: analysis with three-dimensional MR imaging. Osteoarthritis Cartilage 2001;9:101–11.

16. Cicuttini F, Forbes A, Asbeutah A, Morris K, Stuckey S. Comparison and reproducibility of fast and conventional spoiled gradient-echo magnetic resonance sequences in the determination of knee cartilage volume. J Orthop Res 2000;18:580–4.
17. Cicuttini FM, Forbes A, Yuanyuan W, Rush G, Stuckey SL. Rate of knee cartilage loss after partial meniscectomy. J Rheumatol 2002;29:1954–6.
18. Glaser C, Faber S, Eckstein F, *et al.* Optimization and validation of a rapid high-resolution T1-w 3D FLASH water excitation MRI sequence for the quantitative assessment of articular cartilage volume and thickness. Magn Reson Imaging 2001;19:177–85.
19. Disler DG, McCauley TR, Kelman CG, *et al.* Fat-suppressed three-dimensional spoiled gradient-echo MR imaging of hyaline cartilage defects in the knee: comparison with standard MR imaging and arthroscopy. AJR 1996;167:127–32.
20. Cohen ZA, McCarthy DM, Kwak SD, *et al.* Knee cartilage topography, thickness, and contact areas from MRI: *in-vitro* calibration and *in-vivo* measurements. Osteoarthritis Cartilage 1999;7: 95–109.
21. Peterfy CG, White D, Tirman P, *et al.* Whole-organ evaluation of the knee in osteoarthritis using MRI, XIV European League Against Rheumatism Congress, Glasgow, Scotland, June, 1999. Ann Rheum Dis: 38.
22. Drapé J-L, Pessis E, Auleley G, Chevrot A, Dougados M, Ayral X. Quantitative MR imaging of chondropathy in osteoarthritic knees. Radiology 1998;208:49–55.
23. Ayral X. Quantitative arthroscopy. Baillieres Clin Rheumatol 1996;10:477–94.
24. Dardizinski B, Mosher T, Li S, Van Slyke M, Smith M. Spatial variation of T2 in human articular cartilage. Radiology 1997;205:546–50.
25. Mosher T, Dardzinski B, Smith M. Human articular cartilage: influence of aging and early symptomatic degeneration on the spatial variation of T2—preliminary findings at 3 T. Radiology 2000;241: 259–66.
26. Xia Y, Moody JB, Burton-Wurster N, Lust G. Quantitative in situ correlation between microscopic MRI and polerized light microscopy studies of artcular cartilage. Osteoarthritis Cart 2001;9:393–406.
27. Zaim S, Peterfy CG, Lynch JA, Li J, Genant HK. Early cartilage degeneration of the knee after meniscal surgery: MRI findings. Osteoarthritis Cart 2001;9: S37.
28. Peterfy C. Cartilage Changes in Osteoarthritis. In: Haskall V, Dieppe P. eds. The Many Faces of Osteoarthritis: Birkhäuser Verlag, 2002: 329–350.
29. Altman RD, Hochberg M, Murphy WAJ, Wolfe F, Lequesne M. Atlas of individual radiographic features in osteoarthritis. Osteoarthritis Cart 1996;3(suppl. A): 3–70.
30. McQueen FM, Benton N, Crabbe J, *et al.* What is the fate of erosions in early rheumatoid arthritis? Tracking individual lesions using x-rays and magnetic resonance imaging over the first two years of disease. Ann Rheum Dis 2001;60:859–68.
31. Peterfy C, Dion E, Miaux Y, *et al.* Comparison of MRI and X-ray for monitoring erosive changes in rheumatoid arthritis. Arthritis Rheum 1998;41(Suppl):S51.
32. Lindegaard H, Vallø J, Høslev-Petersen K, Junker P, Østergaard M. Low field dedicated magnetic resonance imaging in untreated rheumatoid arthritis of recent onset. Ann Rheum Dis 2001;60:770–6.
33. Backhaus M, Burmester GR, Sandrock D, *et al.* Prospective two year follow up study comparing novel and conventional imaging procedures in patients with arthritic finger joints. Ann Rheum Dis 2002;61: 895–904.
34. Østergaard M, Gideon P, Sorenson K, *et al.* Scoing of synovial membrane hypertrophy and bone erosions by MR imaging and clinically active and inactive rheumatoid arthritis of the wrist. Scand J Rheumatol 1995;24:212–8.
35. Peterfy CG. Medial knee pain in the aging patient. In: Klippel J, Dieppe P, Eds. Rheumatology 2E. Philadelphia: Mosby 1998;8.12.8–9.
36. Felson D, McLaughlin S, Goggins J, *et al.* Bone marrow edema (BME) and its relation to x-ray progression in knee osteoarthritis (OA). Arthritis Rheum 2003;46:S558.
37. Murphy W. Osteomyelitis, septic arthritis and soft tissue infection. In: Resnick D, Ed. Bone and Joint Imaging. Philadelphia: W.B. Saunders 1989;120–35.
38. Zanetti M, Bruder E, Romero J, Hodler J. Bone marrow edema pattern in osteoarthritic knees: correlation between MR imaging and histologic findings. Radiology 2000;215:835–40.
39. Peterfy CG. Imaging of the disease process. Curr Opin Rheumatol 2002;14:590–6.
40. Englund M, Roos EM, Roos HP, Lohmander LS. Patient-relevant outcomes fourteen years after meniscectomy: influence of type of meniscal tear and size of resection. Rheumatology (Oxford) 2001;40: 631–9.
41. Roos EM, Ostenberg A, Roos H, Ekdahl C, Lohmander LS. Long-term outcome of meniscectomy: symptoms, function, and performance tests in patients with or without radiographic osteoarthritis compared to matched controls. Osteoarthritis Cartilage 2001;9: 316–24.
42. Gale DR, Chaisson CE, Totterman SM, Schwartz RK, Gale ME, Felson D. Meniscal subluxation: association with osteoarthritis and joint space narrowing. Osteoarthritis Cartilage 1999;7:526–32.
43. Messner K, Fahlgren A, Persliden J, Andersson BM. Radiographic joint space narrowing and histologic changes in a rabbit meniscectomy model of early knee osteoarthrosis. Am J Sports Med 2001;29: 151–60.
44. Adams J, McAlindon T, Dimasi M, Carey J, Eustace S. Contribution of meniscal extrusion and cartilage loss to joint space narrowing in osteoarthritis. Clin Radiol 1999;54:502–6.
45. Kawahara Y, Uetani M, Fuchi K, Eguchi H, Hashmi R, Hayashi K. MR assessment of meniscal movement during knee flexion: correlation with the severity of cartilage abnormality in the femorotibial joint. J Comput Assist Tomogr 2001;25:683–90.
46. Beltran J, Shankman S. The menisci. In: Davies AM, Cassa-Pullicino VN, Eds. Imaging of the Knee. New York: Springer-Verlag 2002;129–52.
47. Roos H, Adalberth T, Dahlberg L, Lohmander LS. Osteoarthritis of the knee after injury to the anterior cruciate ligament or meniscus: the influence of time and age. Osteoarthritis Cartilage 1995;3:261–7.
48. Smith GN, Mickler EA, Albrecht ME, Myers SL, Brandt KD. Severity of medial meniscus damage in the

canine knee after anterior cruciate ligament transection. Osteoarthritis Cartilage 2002;10:321–6.
49. Ho C. The cruciate and collateral ligaments. In: Davies AM, Cassa-Pullicino VN, Eds. Imaging of the Knee. New York: Springer-Verlag 2002;153–63.
50. Erickson SJ, Prost RW, Timins ME. The 'magic angle' effect: background physics and clinical relevance. Radiology 1993;188:23–5.
51. Rubenstein JD, Kim JK, Morava-Protzner I, Stanchev PL, Henkelamn RM. Effects of collagen orientation on MR imaging characteristics of bovine cartilage. Radiology 1993;188:219–26.
52. Peterfy CG, Janzen DL, Tirman PFJ, van Dijke CF, Pollack M, Genant HK. Magic-angle phenomenon: a cause of increased signal in the normal lateral meniscus on short-TE MR images of the knee. AJR 1994;163:149–54.
53. Fernandez-Madrid F, Karvonen RL, Teitge RA, Miller PR, An T, Negendank WG. Synovial thickening detected by MR imaging in osteoarthritis of the knee confirmed by biopsy as synovitis. Magn Reson Imaging 1995;13:177–83.
54. Brandt KD. Insights into the natural history of osteoarthritis and the potential for pharmacologic modification of the disease afforded by study of the cruciate-deficient dog. In: Keutner KE, Goldberg VM, Eds. Osteoarthritic Disorders. Rosemont, IL: American Acadamy of Orthopaedic Surgeons 1995;419–26.
55. Peterfy CG, Majumdar S, Lang P, van Dijke CF, Sack K, Genant H.. MR imaging of the arthritic knee: improved discrimination of cartilage, synovium and effusion with pulsed saturation transfer and fat-suppressed T1-weighted sequences. Radiology 1994;191:413–9.
56. Palmer WE, Rosenthal DI, Shoenberg OI, *et al.* Quantification of inflammation in the wrist with gadolinium-enhanced MR imaging and PET with 2-[F-18]-fluoro-2-deoxy-D-glucose. Radiology 1995; 196:645–55.
57. König H, Sieper J, Sorensen M, K-J W. Contrast-enhanced dynamic MR imaging in rheumatoid arthritis of the knee joint: follow-up study after cortisol drug therapy, 77th Scientific Assembly and Annual Meeting of the Radiological Society of North America, Chicago, IL, 1991.
58. Yamato M, Tamai K, Yamaguchi T, Ohno W. MRI of the knee in rheumatoid arthritis: Gd-DTPA perfusion dynamics. J Comput Assist Tomogr 1993;17:781–5.
59. Heuck AF, Steiger P, Stoller DW, Glüer CC, Genant HK. Quantification of knee joint fluid volume by MR imaging and CT using three-dimensional data processing. J Comput Assist Tomogr 1989;13: 287–93.
60. Janzen DL, Peterfy CG, Tirman PFJ, Genant HK. Cystic lesions around the knee joint: MR imaging findings. Am J Roentgenol 1994;163:155–61.
61. Morrison JL, Kaplan PA. Water on the knee: cysts, bursae, and recesses. MRI Clinics N Am 2000; 8:349–70.